LETTERS
PUBLISHED ONLINE: 14 AUGUST 2011 | DOI: 10.1038/NPHYS2058

nature physics

Unexpected mass acquisition of Dirac fermions at the quantum phase transition of a topological insulator

T. Sato[1]*, Kouji Segawa[2], K. Kosaka[1], S. Souma[3], K. Nakayama[1], K. Eto[2], T. Minami[2], Yoichi Ando[2]* and T. Takahashi[1,3]

The three-dimensional (3D) topological insulator is a novel quantum state of matter where an insulating bulk hosts a linearly dispersing surface state, which can be viewed as a sea of massless Dirac fermions protected by the time-reversal symmetry (TRS). Breaking the TRS by a magnetic order leads to the opening of a gap in the surface state[1], and consequently the Dirac fermions become massive. It has been proposed theoretically that such a mass acquisition is necessary to realize novel topological phenomena[2,3], but achieving a sufficiently large mass is an experimental challenge. Here we report an unexpected discovery that the surface Dirac fermions in a solid-solution system $TlBi(S_{1-x}Se_x)_2$ acquire a mass without explicitly breaking the TRS. We found that this system goes through a quantum phase transition from the topological to the non-topological phase, and, by tracing the evolution of the electronic states using the angle-resolved photoemission, we observed that the massless Dirac state in $TlBiSe_2$ switches to a massive state before it disappears in the non-topological phase. This result suggests the existence of a condensed-matter version of the 'Higgs mechanism' where particles acquire a mass through spontaneous symmetry breaking.

Whether a band insulator is topological or not is determined by the parity of the valence-band wave function, which is described by the Z_2 topological invariant. Strong spin–orbit coupling can lead to an inversion of the character of valence- and conduction-band wave functions, resulting in an odd Z_2 invariant that characterizes the topological insulator[4,5]. All known topological insulators[6–14] are based on this band-inversion mechanism[4,5,15–18], but the successive evolution of the electronic state across the quantum phase transition (QPT) from trivial to topological has not been well studied in 3D topological insulators owing to the lack of suitable materials. $TlBi(S_{1-x}Se_x)_2$ is therefore the first system where one can investigate the 3D topological QPT (ref. 19). The advantage of this system is that it always maintains the same crystal structure (Fig. 1a), irrespective of the S/Se ratio. Low-energy, ultrahigh-resolution angle-resolved photoemission spectroscopy (ARPES), which has recently become available, is particularly suited to trace such a QPT in great detail.

The bulk band structures of the two end members, $TlBiSe_2$ and $TlBiS_2$, are shown in Fig. 1b, where one can see several common features, such as the prominent hole-like band at the binding energy E_B of 0.5–1 eV and a weaker intensity at the Fermi level (E_F), both being centred at the $\bar{\Gamma}$ point (Brillouin-zone centre). These features correspond to the top of the bulk valence band (VB) and the bottom of the bulk conduction band (CB), respectively, demonstrating that both $TlBiSe_2$ and $TlBiS_2$ samples are originally insulators with a bandgap of 0.3–0.4 eV, but electron carriers are doped in the naturally-grown crystals[10–12]. Besides the wider VB width in $TlBiS_2$, which is naturally expected from its smaller lattice constant, the VB structures in the two systems are very similar (Fig. 1c).

A critical difference in the electronic states of the two compounds is recognized by looking at the band dispersion in the vicinity of E_F around the $\bar{\Gamma}$ point (Fig. 1d). An 'X'-shaped surface band that traverses the bulk bandgap is clearly recognized in $TlBiSe_2$ (ref. 10), whereas such a surface state is completely absent in $TlBiS_2$. This indicates a topologically distinct nature between the two, despite the similar overall bulk band structure. One can thus conclude that the band parity is inverted in $TlBiSe_2$, whereas it is not in $TlBiS_2$.

What would happen if we mixed the topologically non-trivial $TlBiSe_2$ and trivial $TlBiS_2$ phases? One natural consequence of such an alloying would be that the bulk bandgap closes owing to the switching of the parity of the VB wave function at a certain Se content x_c, marking a topological QPT across which the massless Dirac-cone surface band appears (vanishes) once the system enters into the topological (non-topological) phase. The surface band in the topological phase would retain the Kramers degeneracy at the Dirac point and retain the massless character, as long as the alloying disorder does not break the TRS. It turns out that the electronic-structure evolution in $TlBi(S_{1-x}Se_x)_2$ indeed presents the topological QPT, but it bears a feature that is totally unexpected.

Figure 2a shows the near-E_F ARPES intensity around the zone centre for a series of x values, including $TlBiSe_2$ ($x = 1.0$) and $TlBiS_2$ ($x = 0.0$). One can immediately see that the surface state is seen for $x \geq 0.6$, whereas it is absent for $x \leq 0.4$ (see also Supplementary Information), which points to the topological QPT occurring at $x_c \approx 0.5$. In fact, the bulk bandgap estimated from our data approaches zero on both sides of the QPT (see Fig. 3d), suggesting that a band inversion takes place across the QPT, in accordance with the natural expectation and also with a recent ARPES study independently done on $TlBi(S_{1-x}Se_x)_2$ (ref. 19).

The unexpected physics manifests itself at the Dirac point. The bright intensity peak at ~0.4 eV at $x = 1.0$ is no longer visible at $x = 0.9$ and is markedly suppressed at $x = 0.6$, suggesting that the Kramers degeneracy is lifted on S substitution whereas the surface state is still present. In fact, a closer look at the energy-distribution curves (EDCs) in Fig. 2b shows that the originally X-shaped surface

[1]Department of Physics, Tohoku University, Sendai 980-8578, Japan, [2]Institute of Scientific and Industrial Research, Osaka University, Ibaraki, Osaka 567-0047, Japan, [3]WPI Research Center, Advanced Institute for Materials Research, Tohoku University, Sendai 980-8577, Japan.
*e-mail: t-sato@arpes.phys.tohoku.ac.jp; y_ando@sanken.osaka-u.ac.jp.

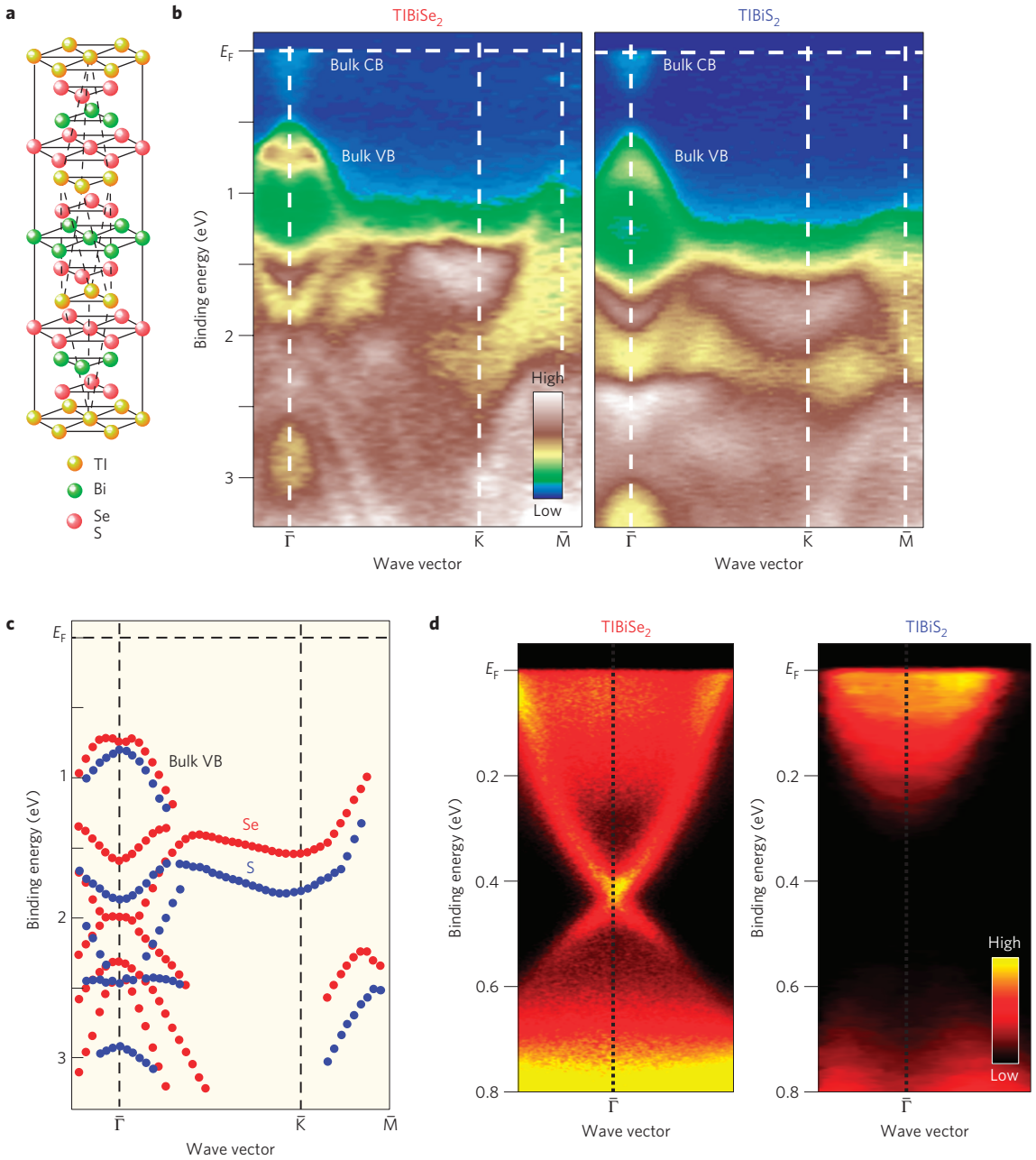

Figure 1 | Comparison of the valence-band structure between $TlBiSe_2$ and $TlBiS_2$. a, Crystal structure of $TlBi(S_{1-x}Se_x)_2$. **b**, Valence-band ARPES intensity along the $\bar{\Gamma}$-$\bar{K}$-$\bar{M}$ direction of the surface Brillouin zone for $TlBiSe_2$ and $TlBiS_2$, plotted as a function of wave vector and binding energy, measured using the He Iα resonance line ($h\nu = 21.218$ eV) at $T = 30$ K. **c**, Direct comparison of the valence-band dispersions between $TlBiSe_2$ and $TlBiS_2$. The energy positions of the bands are determined by tracing the peak position of the second derivatives of the ARPES spectra. Several branches of dispersive bands in both compounds are found at E_B higher than 1 eV; these are attributed to the hybridized states of Tl 6*p*, Bi 6*p* and Se 4*p* (S 3*p*) orbitals[16–18]. Clearly, the bands in $TlBiS_2$ are shifted towards higher E_B with respect to those in $TlBiSe_2$, with the energy shift being more enhanced in deeper-lying bands, indicating the relative expansion of the VB width in $TlBiS_2$. **d**, Comparison of the near-E_F ARPES intensity around the $\bar{\Gamma}$ point between $TlBiSe_2$ and $TlBiS_2$, measured using the Xe I resonance line ($h\nu = 8.437$ eV). The absence of the surface band in $TlBiS_2$ was also confirmed by varying the photon energy and light polarization of the synchrotron radiation.

band at $x = 1.0$, where the EDC at the $\bar{\Gamma}$ point is well fitted by a slightly asymmetric Lorentzian, splits into lower and upper branches at $x = 0.9$, with a finite energy gap at the $\bar{\Gamma}$ point. Further substitution of S results in the reduction and the broadening of the intensity of the surface band (see EDCs for $x = 0.6$), but the energy position of the surface band can be still traced, as illustrated in the second-derivative intensity plots in Fig. 2c. The surface-state nature of this band was confirmed by the stationary nature of its energy position with respect to the photon energy (Supplementary Information), so this band evidently represents massive Dirac fermions on the surface. As a result of the gapped nature, this phase cannot be called topological in the strict sense, but the massive Dirac fermions are obviously of topological origin, suggesting that the bulk bands are kept inverted. On the other hand, the photon-energy dependence of the ARPES spectra for $x = 0.4$ signifies the absence of the surface state, in contrast to the clear signature of it for $x = 0.6$ (Supplementary Information). The disappearance of the surface state and the very narrow bulk gap at $x = 0.4$ (which can be inferred

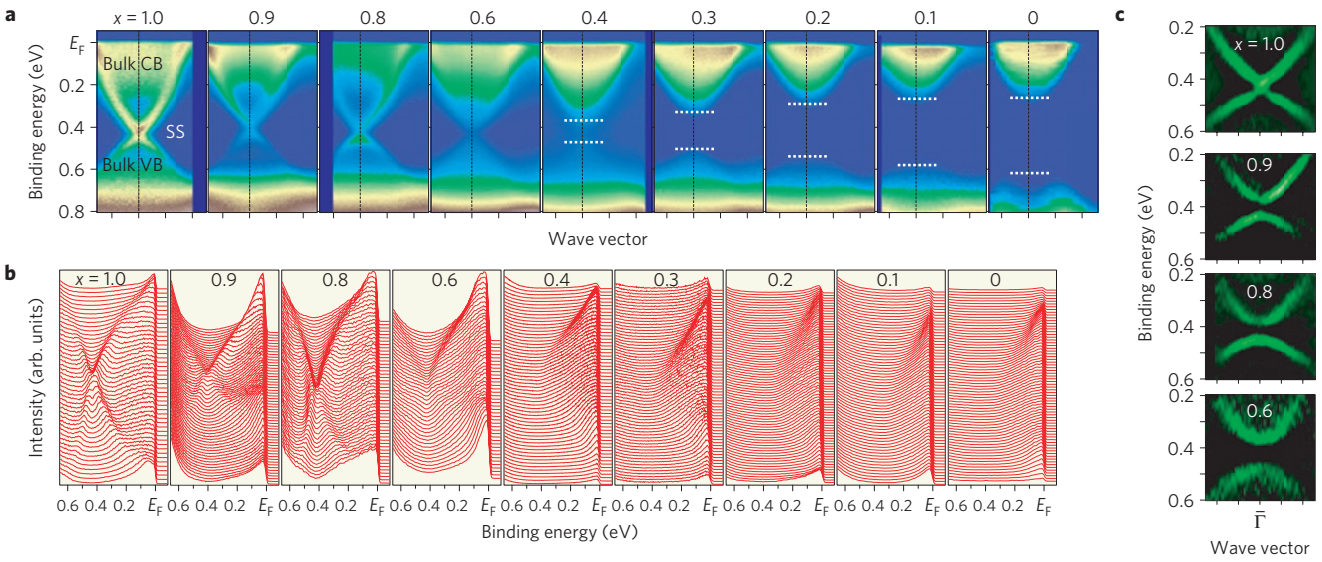

Figure 2 | Mass acquisition of surface Dirac fermions in $TlBi(S_{1-x}Se_x)_2$. **a**, Near-E_F ARPES intensity around the $\bar{\Gamma}$ point as a function of wave vector and binding energy in $TlBi(S_{1-x}Se_x)_2$ for a series of Se concentrations, measured using the Xe I line with the same experimental geometry. White dotted lines for $x \leq 0.4$ represent the top of the VB and the bottom of the CB, thus highlighting the bandgap; owing to the k_z dispersion of the bulk bands, the true gap is likely to be smaller than these estimates, as is reflected in the error bars in Fig. 3d. **b**, Energy distribution curves (EDCs) of the data shown in **a**. **c**, Second-derivative plots of the ARPES intensity for $x = 1.0$, 0.9, 0.8 and 0.6.

from Supplementary Fig. S2) point to the topological QPT being located between $x = 0.6$ and 0.4. Interestingly, the surface bandgap, called here the Dirac gap, grows with decreasing x (less than 0.1 eV at $x = 0.9$ and 0.8, and greater than 0.1 eV at $x = 0.6$), indicating that the S content is closely related to the magnitude of the Dirac gap. We also found that the magnitude of the Dirac gap does not diminish with increasing temperature (Supplementary Information), which argues against a magnetic-order origin of the gap. We note that in a recent independent work[19] the Dirac cone was reported to remain gapless for $x > 0.5$, in contrast to the gapped surface states for $0.6 \leq x \leq 0.9$ observed here. This discrepancy may be due to the difference in the energy resolution (15 meV in ref. 19, as opposed to 2–4 meV in the present experiment).

One may wonder if the bulk bandgap really closes at $x_c \approx 0.5$. If the bandgap never closes, the samples for both $x = 1.0$ and 0.0 should be in the same topological phase. Apparently, this is inconsistent with our ARPES data in Fig. 1d. According to the fundamental principle of the topological band theory, the QPT must always be accompanied by a bandgap closing. Hence, based on our data, the bandgap closing must be happening either at $0.4 < x < 0.6$ or at $0.9 < x < 1.0$ (at which the Dirac gap starts to open). Taking into account the gradual reduction of the bandgap size on approaching $x = 0.5$, it is most sensible to conclude that the inevitable closing of the gap takes place at $x = 0.5$.

One may also question if the observed Dirac gap might be an artefact of an inhomogeneous S distribution in the sample. To address this question, we employed electron-probe microanalysis (EPMA) on the surface and found that our crystals are exceedingly homogeneous (Supplementary Information). The persistently narrow X-ray diffraction peaks, together with a systematic change of the lattice constants, further corroborate this conclusion (Supplementary Information).

To quantify the magnitude of the Dirac gap, we use the theoretical surface-band dispersion to account for the finite mass term[20] (which was originally proposed to explain the Bi_2Se_3 ultrathin-film data[21]) and numerically simulate the experimentally obtained surface band dispersion near the $\bar{\Gamma}$ point; although the origin of the mass term in $TlBi(S_{1-x}Se_x)_2$ is not clear at the moment. As shown in Fig. 3a, the simulated curves reasonably well reproduce the experimental data, and the obtained Dirac gaps for $x = 0.9$, 0.8 and 0.6 are 50 ± 10, 70 ± 10 and 130 ± 20 meV, respectively. The evolution of the massive Dirac cone is schematically illustrated in 3D images of the band dispersions in Fig. 3b. We have confirmed that the obtained sizes of the Dirac gap are highly reproducible by measuring more than five samples for each composition and also by varying the incident photon energy. Taking into account that all the elements contained in $TlBi(S_{1-x}Se_x)_2$ are nonmagnetic and also that the sample shows no obvious magnetic order (Supplementary Information), our result is a strong indication that the substitution of Se with S in $TlBi(S_{1-x}Se_x)_2$ leads to an unconventional mass acquisition of the surface Dirac fermions without explicitly breaking the TRS.

Based on the present ARPES results, one may draw the electronic phase diagram of $TlBi(S_{1-x}Se_x)_2$, as shown in Fig. 3d. The massless Dirac topological phase is achieved only near $x = 1.0$. Once a small amount of S is substituted for Se, the Dirac gap opens, growing almost linearly as a function of the S content, 1-x. Such a massive Dirac phase is present until the topological QPT occurs at $x_c \approx 0.5$, where the bulk gap closes and the band parity is interchanged.

The mass acquisition of the Dirac fermions indicates that the Kramers degeneracy is lifted, which means that the TRS must be broken on the surface. Given that there is no explicit TRS breaking, the only possibility is that a spontaneous symmetry breaking takes place on the S substitution, which is reminiscent of the Higgs mechanism in particle physics. Therefore, $TlBi(S_{1-x}Se_x)_2$ may serve as a model system to bridge condensed-matter physics and particle physics. The exact mechanism of the mass acquisition is not clear at the moment, but an interesting possibility is that it originates from some exotic many-body effects that can lead to an electronic order, although a simple mechanism like the spin-density wave does not seem to be relevant (Supplementary Information). When the top and bottom surface states coherently couple and hybridize, a Dirac gap can open[21], but the sufficiently large thickness ($>10\,\mu m$) of our samples precludes this origin. Another possibility is that critical fluctuations associated with the QPT are responsible for the mass acquisition, but it is too early to speculate along this line. From the application point of view, the Dirac gap can be much larger than that of the

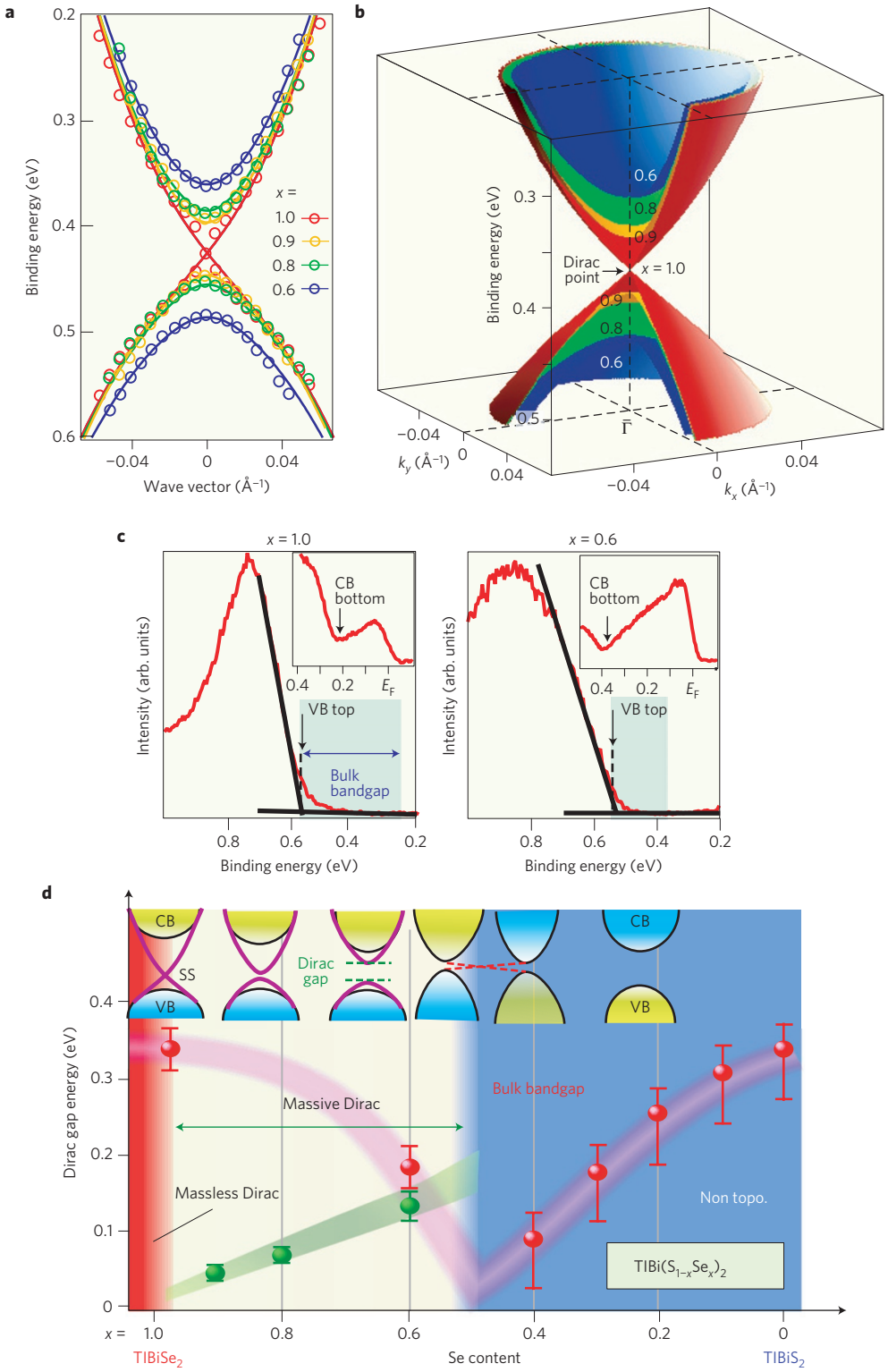

Figure 3 | Massive Dirac fermions and the electronic phase diagram across the topological quantum phase transition. a, Numerical fittings of the ARPES-determined surface band dispersions (open circles) using the theoretical band dispersion which incorporates the finite mass term[20]. Note that the Dirac energy for $x = 0.9$ is shifted downward by 0.015 eV for clarity. **b**, Schematic 3D image of the surface Dirac cone and its energy-gap evolution at low sulphur concentrations. **c**, ARPES spectra around the VB and CB edges for $x = 1.0$ and 0.6, which are used for the bandgap determination for $x > 0.5$, as was done in ref. 10; the photon energies of the synchrotron radiation were chosen to optimally probe the VB top and the CB bottom respectively[10]. **d**, Electronic phase diagram of $TlBi(S_{1-x}Se_x)_2$ showing the surface Dirac gap (green symbols) and the bulk bandgap (red symbols), together with a schematic picture of the band evolution (top) summarizing the present ARPES experiment. Error bars for the Dirac gap energy correspond to the experimental uncertainty in determining the energy position of the band dispersion at the $\bar{\Gamma}$ point in **a**, whereas those for the bulk bandgap originate from the experimental uncertainty in determining the energy difference between the top of the valence band and the bottom of the conduction band in Figs 2 and 3c.

magnetically doped topological insulator Bi_2Se_3 (ref. 1) and is tunable by means of the S/Se ratio, making the $TlBi(S_{1-x}Se_x)_2$ system a prime candidate for device applications that require a gapped surface state.

Methods

High-quality single crystals of $TlBi(S_{1-x}Se_x)_2$ were grown by a modified Bridgman method (see Supplementary Information for details). X-ray diffraction measurements indicated the monotonic shrinkage of *a* and *c* axis lengths on substitution of S for Se, without any apparent change in the relative atomic position with respect to the unit cell. ARPES measurements were performed at Tohoku University using VG-SCIENTA SES2002 and MBS-A1 spectrometers with high-flux He and Xe discharge lamps and a toroidal/spherical grating monochromator. The He Iα ($h\nu = 21.218$ eV) line and one of the Xe I ($h\nu = 8.437$ eV) lines[22] were used to excite photoelectrons. Samples were cleaved *in situ* along the (111) crystal plane in an ultrahigh vacuum of 5×10^{-11} torr. The energy resolutions for the measurement of the VB and near-E_F regions were set at 15 and 2–4 meV, respectively. The angular resolution was 0.2°, corresponding to a *k* resolution of 0.007 and 0.004 $Å^{-1}$ for the He Iα and Xe I photons, respectively. The Fermi level of the samples was referenced to that of a gold film evaporated onto the sample holder. A shiny mirror-like surface was obtained after cleaving samples, confirming its high quality.

Received 30 December 2010; accepted 8 July 2011; published online 14 August 2011

References

1. Chen, Y-L. *et al.* Massive Dirac fermion on the surface of a magnetically doped topological insulator. *Science* **329,** 659–662 (2010).
2. Qi, X-L., Hughes, T. L. & Zhang, S-C. Topological field theory of time-reversal invariant insulators. *Phys. Rev. B* **78,** 195424 (2008).
3. Qi, X-L., Li, R-D., Zang, J-D. & Zhang, S-C. Inducing a magnetic monopole with topological surface states. *Science* **323,** 1184–1187 (2009).
4. Bernevig, B. A., Hughes, T. L. & Zhang, S-C. Quantum spin Hall effect and topological phase transition in HgTe quantum wells. *Science* **314,** 1757–1761 (2006).
5. Fu, L. & Kane, C. L. Topological insulators with inversion symmetry. *Phys. Rev. B* **76,** 045302 (2007).
6. König, M. *et al.* Quantum spin Hall insulator state in HgTe quantum wells. *Science* **318,** 766–770 (2007).
7. Hsieh, D. *et al.* A topological Dirac insulator in a quantum spin Hall phase. *Nature* **452,** 970–974 (2008).
8. Xia, Y. *et al.* Observation of a large-gap topological-insulator class with a single Dirac cone on the surface. *Nature Phys.* **5,** 398–402 (2009).
9. Chen, Y. L. *et al.* Experimental realization of a three-dimensional topological insulator, Bi_2Te_3. *Science* **325,** 178–181 (2009).
10. Sato, T. *et al.* Direct evidence for the Dirac-cone topological surface states in ternary chalcogenide $TlBiSe_2$. *Phys. Rev. Lett.* **105,** 136802 (2010).
11. Kuroda, K. *et al.* Experimental realization of a three-dimensional topological insulator phase in ternary chalcogenide $TlBiSe_2$. *Phys. Rev. Lett.* **105,** 146801 (2010).
12. Chen, Y. L. *et al.* Observation of single Dirac cone topological surface state in compounds $TlBiTe_2$ and $TlBiSe_2$ from a new topological insulator family. *Phys. Rev. Lett.* **105,** 266401 (2010).
13. Ren, Z. *et al.* Large bulk resistivity and surface quantum oscillations in the topological insulator Bi_2Te_2Se. *Phys. Rev. B* **82,** 241306 (2010).
14. Xu, Y-S. *et al.* Discovery of several large families of topological insulator classes with backscattering-suppressed spin-polarized single-Dirac-cone on the surface. Preprint at http://arxiv.org/abs/1007.5111 (2010).
15. Zhang, H. *et al.* Topological insulators in Bi_2Se_3, Bi_2Te_3 and Sb_2Te_3 with a single Dirac cone on the surface. *Nature Phys.* **5,** 438–442 (2009).
16. Yan, B. *et al.* Theoretical prediction of topological insulators in thallium-based III-V-VI_2 ternary chalcogenides. *Europhys. Lett.* **90,** 37002 (2010).
17. Lin, H. *et al.* Single-Dirac-cone topological surface states in the $TlBiSe_2$ class of topological semiconductors. *Phys. Rev. Lett.* **105,** 036404 (2010).
18. Hoang, K. & Mahanti, S. D. Atomic and electronic structures of thallium-based III-V-VI_2 ternary chalcogenides: *Ab initio* calculations. *Phys. Rev. B* **81,** 041309(R) (2010).
19. Xu, S-Y. *et al.* Topological phase transition and texture inversion in a tunable topological insulator. *Science* **332,** 560–564 (2011).
20. Lu, H-Z., Shan, W-Y., Yao, W., Niu, Q. & Shen, S-Q. Massive Dirac fermions and spin physics in an ultrathin film of topological insulator. *Phys. Rev. B* **81,** 115407 (2010).
21. Zhang, L. *et al.* Crossover of the three-dimensional topological insulator Bi_2Se_3 to the two-dimensional limit. *Nature Phys.* **6,** 584–588 (2010).
22. Souma, S., Sato, T., Takahashi, T. & Baltzer, P. High-intensity xenon plasma discharge lamp for bulk-sensitive high-resolution photoemission spectroscopy. *Rev. Sci. Instrum.* **78,** 123104 (2007).

Acknowledgements

We thank N. Nagaosa for valuable discussions. We also thank H. Guo, K. Sugawara, M. Komatsu, T. Arakane and A. Takayama for their assistance in the ARPES experiment, and S. Sasaki for the analysis using EPMA. This work was supported by JSPS (KAKENHI 19674002 and NEXT Program), JST-CREST, MEXT of Japan (Innovative Area 'Topological Quantum Phenomena'), AFOSR (AOARD 10-4103), and KEK-PF (Proposal number: 2009S2-005 and 2010G507).

Author contributions

T.S., K.K., S.S., K.N., and T.T. performed ARPES measurements. K.S. K.E, T.M. and Y.A. carried out the growth of the single crystals and their characterizations. T.S., K.S. and Y.A. conceived the experiments and wrote the manuscript.

Additional information

The authors declare no competing financial interests. Supplementary information accompanies this paper on www.nature.com/naturephysics. Reprints and permissions information is available online at http://www.nature.com/reprints. Correspondence and requests for materials should be addressed to T.S. or Y.A.